RP Materials: Proceedings
Vol. 1, Part 1 (2022) pp. 9–12
e-ISSN:

RESEARCH PLATEAU PUBLISHERS

Cite this article: Sanjay, Analysis and modeling of 10.6 µm PIN detector based on mercury-cadmium-telluride, *RP Materials: Proceedings* Vol. 1, Part 1 (2022) pp. 9–12.

Original Research Article

Analysis and modeling of 10.6 µm PIN detector based on mercury-cadmium-telluride

Sanjay
Department of Physics, G.D.C. Memorial College, Bahal, Bhiwani – 127028, Haryana, India
*Corresponding author, E-mail: sanjay5101979@gmail.com

****Selection and Peer-Review under responsibility of the Scientific Committee of the National Conference on Advanced Engineering Materials (NCAEM 2022).**

ARTICLE HISTORY
Received: 9 Aug. 2022
Revised: 10 Nov. 2022
Accepted: 12 Nov. 2022
Published online: 27 Dec. 2022

KEYWORDS
PIN photodetector; narrow band gap semiconductors; space communication system; MCT.

ABSTRACT
To investigate the device's potential in 10.6 µm optical communication applications, the simplified modeling of the longer-wavelength-Infrared (LWIR) PIN detector dependent on Mercury-Cadmium-Telluride (MCT), narrow band gap semiconductor has been constructed. The current model has been used to analyse and simulate a 77K-operating $Hg_{0.78}Cd_{0.22}Te$ photovoltaic detector. According to theoretical calculations, the diffusing components of device current are subordinate to generation-recombination component. As a result of Auger and Shockley-Read-Hall transitions, the photodetector's performance rating is also influenced by radiative (band to band) and non-radiative recombination. The photodetector displays the following characteristics at 77K: dark current $I = 5\times10^{-7}$ A, dynamic resistance $R = 2.25\times10^{5}$ ohm, quantum efficiency $\eta = 64\%$, and $NEP = 10^{-14}$ W-Hz$^{1/2}$.

1. Introduction

The research and commercial development communities have recently become interested in free space optical communication due to its potential benefits, which include quick deployment times, allotment of channel capacity without licences or fees, minimal power usage, small weight and dimensions, and high efficiency, and no need for a physical medium channel through which information can be transported. Free space optics employs lasers to send data similarly to fiber-based communication, but instead of containing the data stream in a glass fibre, it transmits it over the air. Free space (atmosphere) optical channels, on the other hand, have properties that are very dissimilar from those of fiber-based channels. A number of strategically placed atmospheric attenuation windows are made available to us in the infrared area of the electromagnetic spectrum, allowing for free-space optical communication. Our main focus in the current work is solely on the atmospheric attenuation window at 10.6 µm. Free optical links can be created by directing a CO_2 laser source with a characteristic wavelength of 10.6 µm at receivers for highly sensitive photon detectors to transfer an invisible, eye-safe laser beam from one telescope to another. We discuss our research into a HgCdTe-based photodetector for operation at 10.6 µm at the receiver end in this paper. To theoretically characterise the photodetector for the suggested application, a photodetector simple analytical version has been constructed [1, 2].

2. Device structure and modeling

A p^+-n^0-n^+ homojunction photodetector based on $Hg_{1-x}Cd_xTe$ is the device under discussion. It is suggested that the photodiode be grown on a substrate of lattice-matched CdZnTe. The material's bandgap, which is required to produce the long wavelength cutoff at 10.6 µm, is used to calculate the value of x, the mole fraction Cd in HgCdTe. The intrinsic region, which is somewhat n-type, serves as active layer and receives the incoming radiation from top p^+-layer. The neutral p and intrinsic areas absorb the incident light. As the way to estimate the quantum performance of the photodetector, the current model calls for the solution of a 1-D Poisson's equation under the electromagnetic radiation irradiance. In order to describe the life-time of the carriers, both non-radiative and radiative recombination mechanisms have been taken into account [3]. The applied voltage and incident photon flux both affect the detector's total current. The only factor affecting the diode's current when there is no light coming from it is the bias voltage. The dark currents in the detector are made up of two main parts and are provided by [4].

$$I_D = I_{DIFF} + I_{GR}, \quad (1)$$

where I_{GR} and I_{DIFF} are the generation-recombination and diffusion component of current respectively.

2.1 Diffusion current

This current component involves the dispersion of minority carriers from p+ areas. By solving the 1-D diffusion equation in the absence of light and under suitable boundary conditions, it is possible to determine diffusion current

developed by the minority charge carriers with the bias voltage, V. One may get the diffusion current component by:

$$I_{DIFF} = q\frac{n_i^2 A}{N_d}\frac{D_p}{L_p}\frac{Q_1}{Q_2}.\left(\exp\left(\frac{qV}{kT}\right)-1\right), \tag{2}$$

where

$$Q_1 = \frac{S_p L_p}{D_p}\cosh\left(\frac{d-x_n}{L_p}\right)+\sinh\left(\frac{d-x_n}{L_p}\right)$$

$$Q_2 = \frac{S_p L_p}{D_p}\sinh\left(\frac{d-x_n}{L_p}\right)+\cosh\left(\frac{d-x_n}{L_p}\right).$$

In above equation, D_p is a constant for the holes, L_p is the diffusion length, S_p represents the hole's re-combination speed, d denotes thickness of n^0-regime and A denotes junction area.

2.2 Generation-recombination current

The defects and impurities in the depletion zone which serve as intermediary levels corresponding to thermally generated charge carriers give birth to the generation-recombination current component. Shockley-Read-Hall centres are the names for these transitional stages. Current's generation-recombination component can be roughly described as:

$$I_{GR} = \frac{qn_i AW}{\tau_{SRH}}\frac{2\sinh\left(\frac{qV}{2kT}\right)}{q\left(\frac{V_{bi}-V}{kT}\right)}f(b). \tag{3}$$

In equation (3), n_d represents donor density in n_0 zone, q is electron charge, V_{bi} stands for built-in voltage, V stands for applied potential, W represents thickness of depleted regime (and is a function of applied potential), and other symbols have their usual meanings. The equation for the function $f(b)$, which is dependent on the applied voltage and the trap level E_t, is:

$$f(b) = \int_0^\infty \frac{dx}{x^2+2bx+1} \tag{4a}$$

and

$$b = \exp\left(-\frac{qV}{2kT}\right)\cosh\left[\frac{E_t-E_i}{kT}+\frac{1}{2}\ln(\tau_{SRH})\right]. \tag{4b}$$

The intrinsic Fermi level and trap energy level are represented here by E_t and E_i. The function $f(b)$ has a maximum value of $\pi/2$ at low values of b, and it deviates from this value as b rises.

2.3 Lifetime modeling

This is crucial to predict the life span of minority charge carriers while taking into account all potential recombination mechanisms so as to appropriately predict magnitude of diffusion current's component. Both the non-radiative as well as radiative recombination mechanisms are considered in present analysis. Whereas non-radiative Auger and SRH recombinations involve phonon-assisted transitions, radiative recombination involves photon-assisted band-to-band transfer. In HgCdTe material, the effective lifespan can be calculated as:

$$\frac{1}{\tau_{eff}} = \frac{1}{\tau_R}+\frac{1}{\tau_{AU}}+\frac{1}{\tau_{SRH}}. \tag{5}$$

In equation (5), τ_R, τ_{AU} and τ_{SRH} stand for the lifetimes corresponding to radiative, Auger and SRH recombination mechanisms, respectively.

It has been expected that as distance increases, the optical creation rate of electron-hole pairs will also increase more slowly. The depletion region's photo-generated carriers significantly contribute to overall quantum efficiency, which is roughly expressed as:

$$\eta = (1-R)\left(1-\frac{\exp(-\alpha W)}{1+\alpha L_p}\right), \tag{6}$$

where W is the depletion width.

2.4 Noise-equivalent power (NEP)

NEP, which is the function of quantum efficiency η of LWIR photo-detector for applications in the optical communication system, is a significant figure of merit. It is dependent on wavelength λ of falling infrared radiation. NEP of photo-detector may be measured as root mean square value of optical signal power necessary at the input in order to generate an output, with root mean square signal power comparable to root mean square noise power at output (i.e., S/N = 1 for unit bandwidth). Thus

$$NEP = \frac{(P_{op})_{\min}}{\sqrt{2}}. \tag{7}$$

2.5 Noise current modeling

In the current analysis, it has been considered that incident optical power is intensity modulated, and detector only serves as a photon counter. The expression for the time-dependent incident optical power is [5]:

$$P(t) = P_{op}(1+\mu\exp(j\omega t)), \tag{8}$$

where μ is the index of modulation, P_{op} is the power value of the optical power, and ω (= $2\pi f$) is the modulating angular frequency.

The root-mean-square value of generated signal photocurrent is:

$$i_p = \frac{q\eta\mu P_{opt}}{\sqrt{2}h\nu}. \tag{9}$$

The d.c. current passing through the detector in the presence of illumination has two components, including (i)

dark current caused by thermally generated carriers and (ii) photo-generated current caused by optically generated carriers. Shot noise is a byproduct of the randomness in the creation of these currents. The shot noise current's mean square value can be stated as follows:

$$\left\langle i_s^2 \right\rangle = 2q(I_p + I_D)B\,, \tag{10}$$

where B is the bandwidth, I_p and I_D are the photodetector's dark current and photo-induced current in dc terms, respectively. Moreover, the photo-detector is typically followed by an amplifier step that strengthens the feeble electrical signal it generates. The input resistance of this step is taken into account while calculating noise in the current analysis. The thermal noise current's root mean square value can be stated as follows:

$$\left\langle i_T^2 \right\rangle = \frac{4k_B T}{R_{eq}}, \tag{11}$$

where $\frac{1}{R_{eq}} = \frac{1}{R_D} + \frac{1}{R_B} + \frac{1}{R_L}$.

Here, the photodiode resistance, bias resistor, and input resistance of next amplification stage are all represented by the letters R_D R_B and R_L, respectively. The noise equivalent power corresponding to the specific S/N for 100% modulation (μ = 1) is:

$$NEP = \frac{\sqrt{2}h\nu}{\eta}\left[1+\left\{1+\frac{I_D+\frac{2kT}{qR_{eq}}}{q}\right\}^{/2}\right]. \tag{12}$$

3. Results and discussion

The p_+-$Hg_{0.88}Cd_{0.22}Te$/n^0-$Hg_{0.88}Cd_{0.22}Te$/n^+-$Hg_{0.88}Cd_{0.22}Te$ photo-detector has undergone numerical calculations at 77 K. It has been assumed that the light is coming from the top side of p^+-$Hg_{0.88}Cd_{0.22}Te$. Both the p^+ and n^0 areas absorb incident photons having energies greater than bandgap energy of $Hg_{0.88}Cd_{0.22}Te$. Many parameters are gathered from references [2] and used in numerical calculations.

Figure 1 depicts how the applied voltage affects the diode's dynamic resistance. Our calculations' outcomes demonstrate that G-R current under reverse bias predominantly controls the current in PIN detectors. The diode's zero-bias resistance has been calculated to be 2.25×10^5 Ω.

Figure 2 shows how quantum efficiency varies with operating wavelength. In the targeted 2 μm -10.6 μm area, the quantum efficiency is virtually constant. For applications involving free space optical communication, the proposed device's excellent quantum efficiency at 10.6 μm makes it a desirable option.

Figure 3 depicts how the NEP varies with the wavelength of the incident optical signal. The NEP is very low (= 5×10^{-14} W-$Hz^{1/2}$) for the chosen wavelength region (10.6 μm). As you get into the shorter wavelength region, the NEP grows. Nonetheless, the photo-detector has a low NEP (< 10^{-12} W-$Hz^{1/2}$) over the entire wavelength range (2 - 10.6 μm), making it appropriate for use throughout the entire region. The detector has a peak detectivity of 1.6×10^{10} m$Hz^{1/2}$/W around 10.6 μm and lowest NEP is obtained close to long wavelength cut-off.

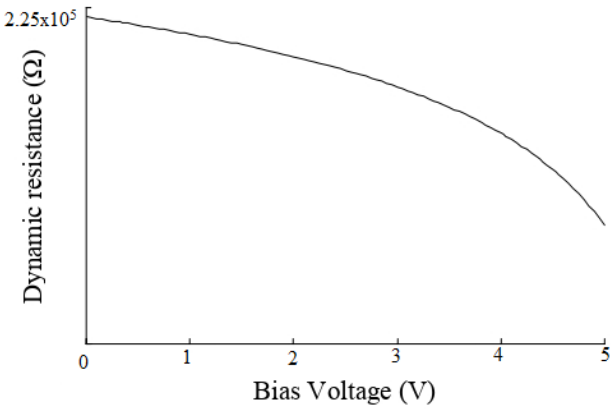

Figure 1: Nature of dependence of dynamic resistance on bias voltage.

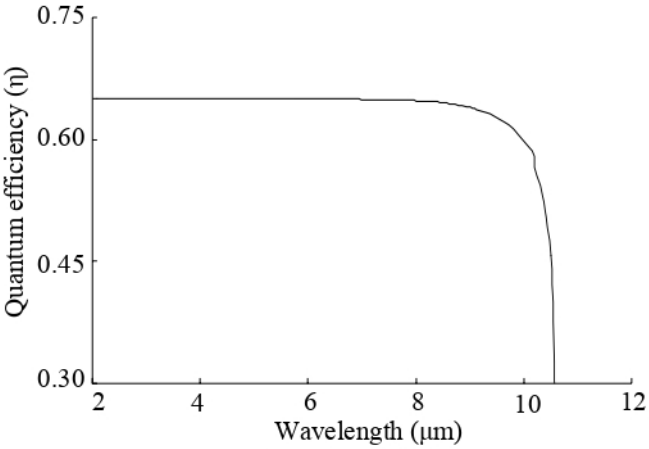

Figure 2: Nature of dependence of quantum efficiency on operating wavelength.

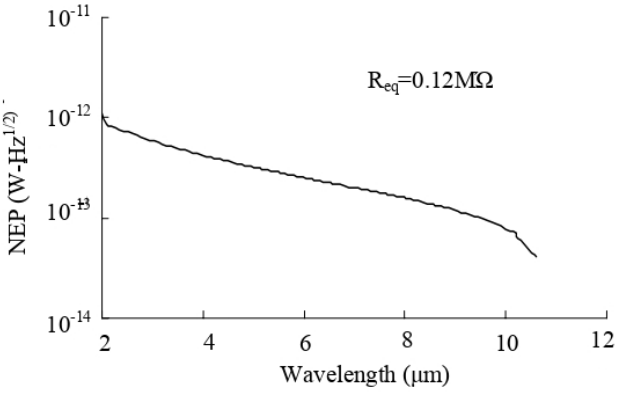

Figure 3: Nature of dependence of NEP on wavelength.

Figure 4 depicts change of noise equivalent power with respect to equivalent resistance. The contribution of thermal noise is observed to be significant when the equivalent resistance is less than 0.1 MΩ, and as a result the detector

exhibits a high value of noise equivalent power. When the equivalent resistance is greater than 0.1 MΩ, the shot noise component takes over as the dominant noise component and the thermal noise component becomes negligible (NEP < 5×10^{-14} W-Hz$^{1/2}$).

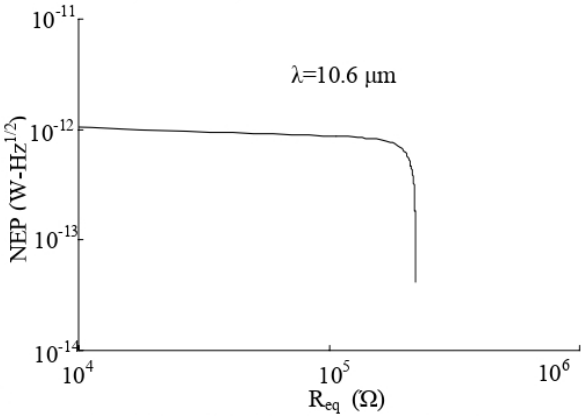

Figure 4: Nature of dependence of NEP on equivalent resistance.

4. Conclusions

The research shows that the proposed photodetector operates at 10.6 μm with a respectably low NEP value. It is anticipated that the photodetector will be used in the needed area of free space optical communication, which operates roughly at the atmospheric window of 10.6 μm. It is feasible to operate the device in an ultra low-noise mode where the shot noise component is the only source of noise by carefully selecting the amplifier design after the detector.

References

[1] H. Melchior, M.B. Fisher, F.R. Arams, Photodetectors for optical communication systems, *Proc. IEEE* **58** (1970) 1466-1476.

[2] A. Rogalski, K. Adamiec, J. Rutkowski, *Narrow-Gap Semiconductor Photodiode*, SPIE Press, Bellingham, USA (2000).

[3] V.C.Lopes, A.J.Syllaios, M.C.Chen, Minority carrier lifetime in mercury cadmium telluride, *Semicond. Sci. Technol.* **8** (1993) 824-841.

[4] P.M. Gorley , M.V. Demych , V.P. Makhniy, Zs. J. Horvath, V.A. Shenderovsky, Current flow mechanisms in p-i-n structures based on cadmium telluride, *Semiconductor Physics, Quantum Electronics & Optoelectronics* **5** (2002) 46.

[5] S.M. Sze, *Physics of Semiconductor Devices*, Wiley Eastern Ltd., New Delhi (1981).